Frontiers of Environmental Science & Engineering
2025, 19(5): 66 https://doi.org/10.1007/s11783-025-1986-7

RESEARCH ARTICLE

Micro-nano bubbles enhanced degradation of emerging contaminants by ferrous-oxalate complexes: synergistic interaction between oxidation and coagulation

Ping Li[1,2,#], Xiaojiang Huang[1,2,#], Qing Yang[3], Haozhe Xia[4], Chunbo Li[1,2], Zhiqiang Zhang[1,2], Xuan Wang[1,2], Jinsuo Lu ✉ [1,2]

1. School of Environmental and Municipal Engineering, Xi'an University of Architecture and Technology, Xi'an 710055, China
2. Key Laboratory of Northwest Water Resources, Environment and Ecology, Ministry of Education, Xi'an 710055, China
3. Ministry of Education Engineering Research Center of Water Resource Comprehensive Utilization in Cold and Arid Regions, Lanzhou 730070, China
4. Xi'an Municipal Water Supply Co., Xi'an 710055, China

HIGHLIGHTS

- The superior oxygenation capacity of MNB greatly improved pollutants degradation.
- Degradation kinetics of BPS depended on the speciation of Fe^{2+}-oxalate complexes.
- Fe^{2+}-oxalate activated O_2 to yield ·OH by one and two electron transfer pathways.
- MNBs boosted ROS formation while promoting iron hydroxide complexes generation.

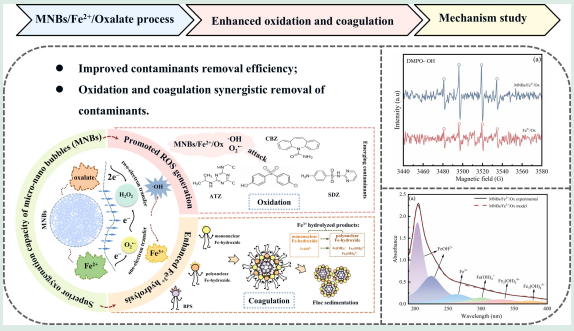

ABSTRACT: The activation of oxygen by ferrous (Fe^{2+}) to generate ·OH for contaminants degradation was inhibited due to the low utilization of oxygen, thus limiting its application in the practical environment. In this study, with the superior oxygenation capacity of micro-nano bubbles (MNBs) and the stronger O_2 activation capacity of Fe^{2+}-oxalate complexes, the MNBs/Fe^{2+}/oxalate (Ox) system was constructed with 4,4′-sulfonyldiphenol (BPS) as the main target emerging contaminants (ECs), and to investigate the enhancement contribution and reinforcement mechanism of the involvement of MNBs to the removal efficiency of ECs in the Fe^{2+}/Ox system. It was shown that the MNBs/Fe^{2+}/Ox system could effectively degrade four structurally diverse ECs. In this case, with BPS as the main target contaminant, adding MNBs could increase the BPS removal efficiency by about 35%. In the MNBs/Fe^{2+}/Ox system, the degradation rate of BPS depended on the concentration of $Fe^{II}(Ox)_2^{2-}$, while the extent of degradation was mainly governed by $Fe^{II}(Ox)_2^{2-}$ and $Fe^{II}(Ox)^0$. EPR and probe experiments showed that the reactive oxygen species (ROS) produced by the system and the iron

✉ Corresponding author. E-mail: lujinsuo@xauat.edu.cn

# These authors contributed equally to this work.

Article history: Received 12 November 2024, Revised 14 February 2025, Accepted 16 February 2025, Available online 24 March 2025

hydroxide complexes produced by Fe^{3+} hydrolysis contributed to the degradation of BPS by oxidation and coagulation, respectively. In particular, ·OH and $O_2^{\bullet -}$ were the main reactive oxygen species produced by this system. Moreover, the involvement of MNBs significantly increased the formation of ROS and iron hydroxide complexes in the Fe^{2+}/Ox system. The oxygenation process of MNBs used in this study enhanced the contaminants degradation performance of the Fe^{2+}/Ox system and has broadened the application scope of MNBs.

KEYWORDS: Micro-nano bubbles, Ferrous, Molecular oxygen activation, Enhanced oxidation, Synergistic interaction

1 Introduction

The hydroxyl radical (·OH) is the strongest reactive oxygen species (ROS) in nature and can non-selectively degrade the vast majority of contaminants (Tong et al., 2016). In addition, ·OH can induce free radical chain reaction, which is especially suitable for removing difficult-to-degrade contaminants (Page et al., 2013; Chen et al., 2021; 2022). In recent years, more and more studies have shown that Fe^{2+} can be used for contaminant degradation by activating O_2 to produce other ROS such as ·OH (Minella et al., 2015; Tong et al., 2016; Zhang et al., 2019). Based on previous studies, it was confirmed that the mechanism of Fe^{2+} activation of O_2 to generate ROS is divided into two types (Keenan and Sedlak, 2008a; Zhang et al., 2019; 2022): 1) one-electron transfer mechanism: Fe^{2+} can first activate O_2 to form superoxide radicals ($O_2^{\bullet -}$), which continue to be reduced by Fe^{2+} to form H_2O_2 (Eqs. (1) and (2)); 2) two-electron transfer mechanism: Fe^{2+} directly reduces O_2 to form H_2O_2 (Eq. (3)). The H_2O_2 generated through both pathways continues to react with Fe^{2+} to generate ·OH (Eq. (4)). However, the ability of Fe^{2+} alone to activate O_2 is very limited and the ROS yield is too low for direct application in environmental remediation.

$$Fe^{2+} + O_2 \rightarrow Fe^{3+} + O_2^{\bullet -} \quad (1)$$

$$Fe^{2+} + O_2^{\bullet -} + 2H_2O \rightarrow Fe^{3+} + H_2O_2 + 2OH^- \quad (2)$$

$$2Fe^{2+} + O_2 + 2H_2O \rightarrow 2Fe^{3+} + H_2O_2 + 2OH^- \quad (3)$$

$$H_2O_2 + Fe^{2+} \rightarrow \cdot OH + Fe^{3+} + OH^- \quad (4)$$

ROS production in the Fe^{2+}/O_2 system can be significantly promoted by the additional addition of oxygenated ligands. So far, the present studies have shown that organic ligands (such as ethylenediaminetetraacetic acid (EDTA) (Noradoun and Cheng, 2005; Belanzoni et al., 2009; Zhou et al., 2014; Fan et al., 2015), citrate (Luo et al., 2009; Lee et al., 2014; Jones et al., 2015; Xie et al., 2021), tartaric acid (Villegas-Guzman et al., 2017; Coleman et al., 2020; Ouyang et al., 2020) and oxalate (Ox) (Keenan and Sedlak, 2008b; Luo et al., 2009; Lee et al., 2014) can significantly increase the capacity of Fe^{2+} to activate O_2. The main reaction mechanism is that the ligand forms ferrous complexes with Fe^{2+} to improve the electron utilization efficiency of Fe^{2+} (Xie et al., 2021), decrease the redox potential of Fe^{2+}/Fe^{3+} while inhibiting the precipitation of iron ions (Keenan and Sedlak, 2008b), and significantly promote the production of ROS. Compared to citrate, EDTA, malonate, and glyoxalate, oxalate has higher reducing power and lower ·OH reactivity (Lee et al., 2014) so that it does not significantly compete with the target contaminant, thus avoiding significant consumption of active species. In addition, the Fe^{2+}-oxalate system activates O_2 more than the Fe^{2+}-citrate system and the Fe^{2+}-EDTA system (Luo et al., 2009), which further promotes the generation of active species based on efficiently enhancing the utilization of O_2.

Molecular oxygen is a green and very potential oxidizer. However, under natural environmental conditions, directly oxidizing contaminants with molecular oxygen is challenging because of spin-forbidden reactions (Metz and Solomon, 2001). However, the activation of molecular oxygen is possible through physical, chemical, and biological methods. By breaking the spin-forbidden reaction, reactive oxygen species (ROS) are generated to effectively degrade contaminants (Anglada et al., 2015; Wu et al., 2020; Li and Li, 2021; Sun et al., 2024). In recent years, micro-nano bubbles (MNBs) have shown significant advantages and development potential in water treatment processes (Agarwal et al., 2011; Li et al., 2014; Wang et al., 2024a) due to their features such as long residence time in the water, large specific surface area, and relatively high transfer efficiency (Zimmerman et al., 2011; Atkinson et al., 2019; Haris et al., 2020). Compared to conventional aeration, MNBs are a more effective water oxygenation

technology due to their efficient mass transfer capabilities (Haris et al., 2020; Sakr et al., 2022). Though MNBs are broadly utilized in water treatment as an environmentally friendly process, few studies related to MNBs with Fe^{2+}-ligand have been conducted until now. Suppose the MNBs aeration technology is applied to the Fe^{2+}-ligand system. In that case, the superior oxygenation performance of MNBs is not only expected to increase the production of ROS to enhance oxidation but also has the potential to promote the formation of Fe^{3+} to enhance coagulation.

The widespread presence of emerging contaminants (ECs) in water has become a severe concern to water safety and human health (Schwarzenbach et al., 2006; Frankowski et al., 2021). ROS have been reported to be advantageous in promoting the degradation of new pollutants based on their strong oxidizing ability (Li et al., 2022; Wang et al., 2024b). In this study, oxalate was chosen as a ligand for Fe^{2+}, and MNBs were combined with the Fe^{2+}/Ox system to enhance O_2 utilization and ROS generation. Because Fe^{3+} produced by the oxidation of Fe^{2+} in the Fe^{2+}/O_2 system can also be used as a coagulant, the addition of MNBs is not only able to increase the concentration of dissolved oxygen (DO) but also expected to have the enhanced efficiency of coagulation. The ability of the MNBs/Fe^{2+}/Ox system to deal with ECs was explored. The mechanisms of ROS generation and BPS degradation were analyzed using free radical scavengers and probe compounds. The effects of diverse environmental factors on the degradation of BPS by this system were evaluated. Finally, the degradation pathway of BPS in the MNBs/Fe^{2+}/Ox system was analyzed. This study was supposed to offer supportive data and a theoretical basis for the practical engineering application of MNBs/Fe^{2+}/Ox system.

2 Materials and methods

2.1 Reagents

All chemicals used in this study were analytical grade, except for acetonitrile and methanol, which were of HPLC grade. 4,4′-sulfonyldiphenol (BPS, $C_{12}H_{10}O_4S$), sulfadiazine (SDZ, $C_{10}H_{10}N_4O_2S$), carbamazepine (CBZ, $C_{15}H_{12}N_2O$), atrazine (ATZ, $C_8H_{14}ClN_5$), p-hydroxybenzoic acid (p-HBA, $C_7H_6O_3$), 1,4-benzoquinone (PBQ, $C_6H_4O_2$), 2,2,6,6-Tetramethylpiperidine 1-oxyl (TEMPO, > 97%), Nitroblue tetrazolium chloride (NBT, $C_{40}H_{30}N_{10}O_6 \cdot 2Cl$), Methyl phenyl sulfoxide (PMSO, C_7H_8OS) and Methyl phenyl sulphone ($PMSO_2$, $C_7H_8O_2S$) were analytical standard reagents obtained from Aladdin Industrial Co., Ltd., Shanghai, China. Ferrous sulfate ($FeSO_4 \cdot 7H_2O$), sodium oxalate (Ox, $Na_2C_2O_4$), hydroxylamine hydrochloride, tert-butanol (TBA, $C_6H_{10}O$), sodium benzoate (BA, $C_7H_5NaO_2$), sodium hydroxide (NaOH), sodium chloride (NaCl), sodium sulfate (Na_2SO_4), sodium nitrate ($NaNO_3$), sodium bicarbonate ($NaHCO_3$), sodium carbonate (Na_2CO_3), calcium chloride ($CaCl_2$), magnesium chloride ($MgCl_2$), sodium acetate anhydrous (CH_3COONa), 1,10-Phenanthroline ($C_{12}H_8N_2 \cdot 4H_2O$), ammonium acetate (CH_3COONH_4) were analytical grade and bought from Sinopharm Chemical Reagent Co., Ltd., Shanghai, China. Humic acid (HA ⩾ 99%), 5,5-dimethyl-1-pyrroline-N-oxide (DMPO, > 97%), and 8-hydroxy-7-iodoquinolinium-5-sulphonate ($C_9H_6INO_4S$, ⩾ 98.5%) were provided by Macklin Biochemicals Ltd., Shanghai, China. In this study, all the solutions used were made up by dissolving the required reagents in deionized water.

2.2 Experimental procedure

The procedure for preparing the BPS and sodium oxalate stock solutions required for the experiment was detailed in Text S1. A model of the experimental setup was shown in Fig. S1. The procedure for this experiment was shown below: 1 mL of BPS stock solution was placed in a 1000 mL jar and a certain amount of sodium oxalate stock solution was added to the BPS solution, and then the experiment was run on a magnetic stirrer. The micro-nano bubble generator then generated MNBs in solution at an inlet flow rate (Q_g) of 10 mL/min. After the micro-nano bubbles circulated in solution for 90 s, ferrous sulfate was added to initiate a chain reaction. To test the effect of different ROS on contaminants degradation during the reaction, the experiments were conducted using TBA (·OH scavenger) and PBQ ($O_2^{\bullet -}$ scavenger) to observe the changes in the concentration of contaminants. BA was used as a probe to test the concentration of ·OH and the p-HBA produced during the oxidation of BA by ·OH to evaluate the cumulative yield of ·OH. NBT as a probe for the detection of $O_2^{\bullet -}$. Three times were repeated for all experiments to ensure reproducibility.

2.3 Micro-nano bubble generator

The micro-nano bubble generator for the paper was obtained from Shanghai Xingheng Technology Co. (LF-1500, China). MNBs were generated through the dissolved gas method by pressurization. In this study, the micro-nano bubble generator made use of air as the gas source. The pressure inside the micro-nano bubble generator was kept at 0.4 MPa during the experiments

and only the inlet flow rate to the generator was varied (Q_g = 10, 20, 40, 60 mL/min).

2.4 Analytical methods

The concentrations of BPS, SDZ, CBZ, ATZ, PMSO, $PMSO_2$, and p-HBA were tested with an HPLC device (Ultima 3000, Thermo Scientific, USA) (Table S1). The degradation intermediates of BPS were detected by liquid mass spectrometry (LC-MS, Agilent 1260 Infinity II Prime, USA) as detailed in (Text S2). Determination of Fe^{2+} concentration using phenanthroline chromogenic method (Text S3), the total iron (Fe_{tot}) concentration was determined by reducing Fe^{3+} to Fe^{2+} with hydroxylamine hydrochloride, and the Fe^{3+} concentration was computed from the difference between the Fe_{tot} and Fe^{2+} concentrations. Detection of free radical generation by electron paramagnetic resonance (EPR, EPR, ZMXmicro-6/1, Hach, USA) using DMPO and TEMPO as ·OH, $O_2^{\bullet -}$ and $^1O_2$ trapping agent. The species variation of iron in water samples was detected using a UV-visible spectrophotometer (U-3900, Hitachi, Japan), and data were collected in the range of 190–400 nm. The presence and distribution of individual bands of iron species were assessed using deconvolution methods (Text S4) (Yang et al., 2022). The DO concentration of water containing MNBs was measured using a portable dissolved oxygen meter (HQ40d, Hach, USA).

3 Results and discussion

3.1 Optimum oxygenation conditions for MNBs

Figure 1(a) showed the variation of solution dissolved oxygen concentration (DO) at four different inlet flow rates (Q_g = 10, 20, 40, and 60 mL/min) between 0 and 600 s of the micro-nano bubble generator operation. In summary, the DO concentration first rapidly increased with the operation of the MNBs generator and then gradually decreased. During the initial operation phase, the air was compressed into the water. The DO concentration of the water increased rapidly while a large number of MNBs were formed, and the water took on a milky color. After that, with the extended operation time, a large number of MNBs clustered into large bubbles and burst, reducing the DO concentration in the water. Moreover, it was found that the lower the inlet flow rate of the micro-nano bubble generator, the higher the peak DO level, which was 12.98 and 11.90 mg/L at Q_g = 10 and 20 mL/min, which were higher than 10.83 and 10.43 mg/L at Q_g = 40 and 60 mL/min, respectively. Also, DO reached its peak faster at Q_g = 10 and 20 mL/min than at higher intake flow rates Q_g = 40 and 60 mL/min. This is due to the fact that higher inlet rates reduce the ability of the device to generate micro-nano bubbles and also accelerate bubble aggregation and bursting, which in turn reduces the DO content (Zhou et al., 2022). Figure 1(b) showed the variation of DO concentration in water when the DO concentration peaked and the MNBs generator was stopped under different Q_g conditions. The results indicated that the DO content of the water remained relatively stable during the 30 min of standing. Meanwhile, the effect of pH on DO concentration was shown in Fig. 1(c) DO concentration was maximum under neutral conditions, and too high or too low pH affected the bilayer structure of MNBs (Takahashi, 2005). In summary, the optimal oxygenation condition for MNBs was set as Q_g = 10 mL/min, aeration time = 90 s, and pH = 7.

3.2 Degradation of BPS in MNBs/Fe^{2+}/Ox system

The degradation of BPS under different conditions was investigated prior to the batch experiments. As shown

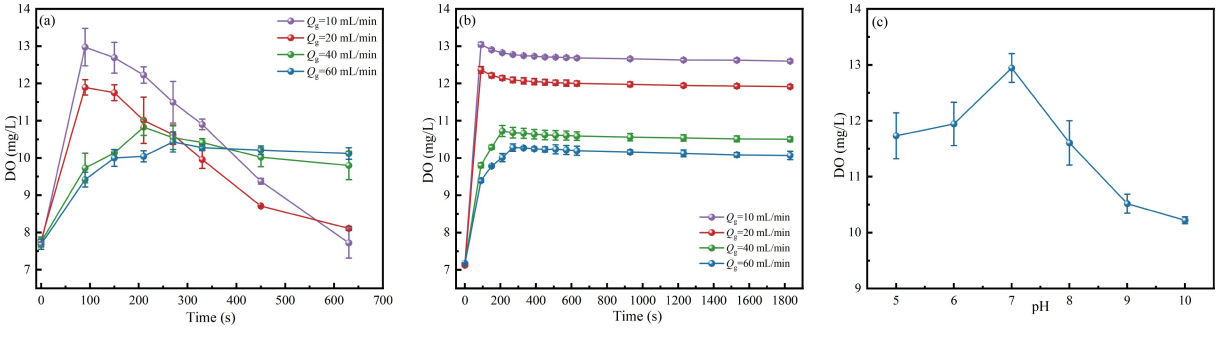

Fig. 1 Results of DO concentration variation with circulation time of MNBs at different Q_g (a); changes of DO concentration in solution at different resting times after the MNBs generator stopped running (b); changes in DO concentration under different pH conditions (c). (pH = 7.0, Q_g = 10 mL/min, t = 90 s).

in Fig. 2(a), Fe^{2+} and oxalate could not alone degrade BPS. The degradation of BPS by MNBs/Fe^{2+} increased to about 10% after the involvement of MNBs, which was attributed to the fact that the addition of MNBs significantly increased the DO concentration of the water. The degradation of BPS in the Fe^{2+}/Ox system was 48% in 120 min. However, after the involvement of MNBs, the degradation efficiency of BPS reached 83% (an increase of about 1.7 times). The addition of MNBs could significantly promote the degradation of BPS by the Fe^{2+}/Ox system.

Furthermore, the changes in DO concentration and pH during the reaction were monitored. As shown in Figs. S2 and S3, the participation of MNBs could significantly increase the concentration of DO in the system, and the DO concentration was consistently higher than the DO concentration in the initial water column throughout the reaction. This further confirmed the superior oxygenation performance of MNBs. The pH value was basically stabilized at about 7, which indicated that the MNBs/Fe^{2+}/Ox system had better stability.

It has been reported that Fe^{2+}/Ox complexes exist mainly as $Fe^{II}(Ox)_2^{2-}$ and $Fe^{II}(Ox)^0$ in water, which can be used to reduce O_2 by one or two-electron transfer reactions (Park et al., 1997; Strathmann and Stone, 2002). In the Fe^{2+}/Ox system, since $Fe^{II}(Ox)_2^{2-}$ has a much smaller reduction potential (E^0) than $Fe^{II}(Ox)^0$ [$E^0(Fe^{III}(Ox)_2^{-}/Fe^{II}(Ox)_2^{2-})$ = + 0.256 V_{NHE} vs $E^0(Fe^{III}(Ox)^{+}/Fe^{II}(Ox)^0)$ = + 0.503 V_{NHE}], so the transfer of electrons from $Fe^{II}(Ox)_2^{2-}$ to O_2 (or H_2O_2) is considerably quicker than $Fe^{II}(Ox)^0$. Therefore, contaminant degradation rates mainly depends on the $Fe^{II}(Ox)_2^{2-}$ concentration (Strathmann and Stone, 2002; Lee et al., 2014). In addition, the extent of contaminant degradation depends on the total concentration of $Fe^{II}(Ox)^0$ and $Fe^{II}(Ox)_2^{2-}$, which can also reduce O_2 and H_2O_2, although $Fe^{II}(Ox)^0$ reacts slowly (Lee et al., 2014).

The degradation of BPS by the MNBs/Fe^{2+}/Ox

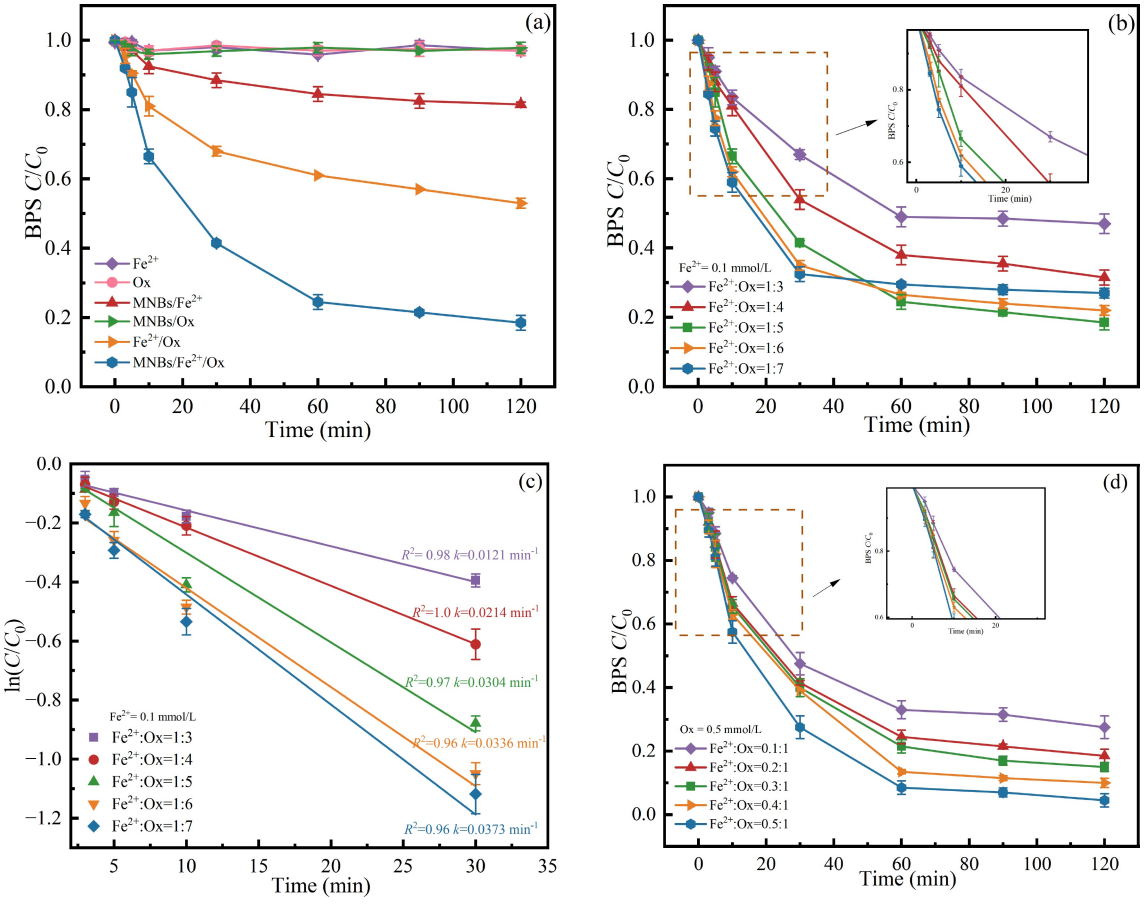

Fig. 2 Degradation of BPS under different conditions (a); influence of oxalate concentration on the degradation of BPS (b); Using a pseudo-first-order kinetic model to calculate the $\ln(C/C_0)$ versus time for k_{obs} (c); influence of Fe^{2+} concentration on the degradation of BPS (d). (pH = 7.0, [Fe^{2+}] = 0.1 mmol/L, [oxalate] = 0.5 mmol/L, BPS = 100 μg/L, Q_g = 10 mL/min, t = 90 s).

system was investigated by varying the ratio of Fe^{2+}/Ox. In this system, the amount of BPS degradation first increased and then declined with increasing oxalate concentration (shown in Fig. 2(b)), which was attributed to the fact that oxalate itself could react with ·OH ($k = 4.7 \times 10^7$ $M^{-1}\cdot s^{-1}$ with $HC_2O_4^-$ and $k = 7.7 \times 10^6$ $M^{-1}\cdot s^{-1}$ with $C_2O_4^{2-}$) (Lee et al., 2014). Under higher oxalate concentrations, excessive oxalate increased the risk of additional consumption of ·OH and thus reduced the oxidation capacity of the reaction system, leading to a decrease in BPS degradation. However, the rate of the BPS degradation increased when the oxalate concentration increased, as shown in Fig. 2(c). That was because oxalate at higher concentrations facilitated the generation of $Fe^{II}(Ox)_2^{2-}$ species, which are more reactive than $Fe^{II}(Ox)^0$ species from a thermodynamic perspective (Strathmann and Stone, 2002). In addition, the E^0 value of the Fe^{2+}/Ox complex in solution decreased with increasing oxalate concentration (Chandra and Jeffrey, 2005). According to Fig. 2(d), when the concentration of oxalate was constant and the concentration of Fe^{2+} varied, the amount of BPS degradation increased with the increase of Fe^{2+} concentration. It was because the increase in Fe^{2+} concentration led to the increase of $Fe^{II}(Ox)^0$ and $Fe^{II}(Ox)_2^{2-}$ concentration, which accelerated oxygen consumption and promoted the degradation of BPS. Except for BPS, the other three emerging contaminants, ATZ, CBZ, and SDZ, were degraded to a certain extent in the MNBs/Fe^{2+}/Ox system (shown in Fig. S4). Therefore, the MNBs/Fe^{2+}/Ox process had universal applicability.

3.3 Degradation mechanism of BPS in MNBs/Fe^{2+}/Ox system

To detect what kinds of ROS were generated in the MNBs/Fe^{2+}/Ox system, the EPR method was first used in this study to determine the types of ROS. The results were shown in Figs. 3(a) and 3(b). Intense four-line ESR signals of DMPO-·OH(1:2:2:1) and DMPO-$O_2^{\bullet -}$(1:1:1:1) were measured in the reaction system with or without the involvement of MNBs. Singlet oxygen($^1O_2$) and Fe(IV) were not observed in this reaction system (Figs. S5 and S6). Besides, the heights of the characteristic peaks in the EPR indicated that the characteristic peaks of ·OH and $O_2^{\bullet -}$ were significantly stronger when MNBs were involved into the system than the system without the involvement of MNBs. The above results demonstrated that the involvement of MNBs significantly boosted the generation of ROS in the Fe^{2+}/Ox system. Meanwhile, the results of detecting the change of ·OH concentration in different systems in Fig. S7 and the momentary concentration variation of $O_2^{\bullet -}$ in the reaction system with or without the involvement of MNBs shown in Fig. S8 agreed with the above conclusion. Next, to further explore the ROS contribution to BPS degradation in the system, TBA ($k_{TBA,\bullet OH} = 6.0 \times 10^8$ $M^{-1}\cdot s^{-1}$) and PBQ ($k_{PBQ,O_2^{\bullet -}} = 9.1 \times 10^8$ $M^{-1}\cdot s^{-1}$) were utilized to capture ·OH and $O_2^{\bullet -}$ (Zhang et al., 2022; 2025). The optimal concentration of scavenger based on the results of numerous trials was shown in Fig. S9. It was shown in Fig. S10 that the scavengers addition prevented the degradation of BPS to various degrees, which provided the essential roles of ·OH and $O_2^{\bullet -}$ on BPS degradation. When both TBA and PBQ were also added to the system, there was just about 18% degradation of BPS, which was attributed to the role of Fe^{3+} coagulation. Figure 3(c) demonstrated the variation of iron content in the Fe^{2+}/Ox system in the presence or absence of MNBs. It could be distinctly concluded that the involvement of MNBs promoted the oxidation of Fe^{2+} and the formation of Fe^{3+}.

The previous studies reported that ·OH production in the Fe^{2+}/O_2 system had both a one-electron transfer mechanism for O_2 and a two-electron transfer mechanism for O_2 (Keenan and Sedlak, 2008a; Zhang et al., 2019; 2022). PBQ was added to eliminate not only the impact of $O_2^{\bullet -}$ but also the subsequent formation of ·OH by a one-electron-transfer route. At this point, the BPS was only degraded by the ·OH produced by the double electron transfer mechanism and coagulation. The addition of TBA eliminated the effect of ·OH produced by both pathways, and the degradation of BPS was mainly a function of $O_2^{\bullet -}$ and coagulation. Therefore, the contribution of one-electron transfer of ·OH could be calculated by subtracting the contribution of $O_2^{\bullet -}$, two-electron transfer of ·OH, and coagulation. Figure 3(d) showed the contribution of ·OH, $O_2^{\bullet -}$ and coagulation to BPS degradation, with oxidation contributing 78% and coagulation 22%.

In addition, Fe^{3+} ions could be readily hydrolyzed to produce positively charged monomer and polymer species. These species have been demonstrated to be the key substances driving coagulation (Jiménez et al., 2012). Therefore, the detection of these substances in the MNBs/Fe^{2+}/Ox system was beneficial for analyzing the enhancement of coagulation by MNBs in this system. Figures 4(a) and 4(b) displayed the UV spectra of the supernatant in the Fe^{2+}/Ox system with and without MNBs, respectively. For each spectrum, six Gaussian bands in the 190–400 nm range, with the peaks at 205 and 220 nm represented $FeOH^{2+}$ mononuclear iron hydroxide complexes; the peak at 260 nm represented Fe^{3+}; and the peaks at 300, 335, and 372 nm represented $Fe(OH)_2^+$, $Fe_2(OH)_2^{4+}$, and

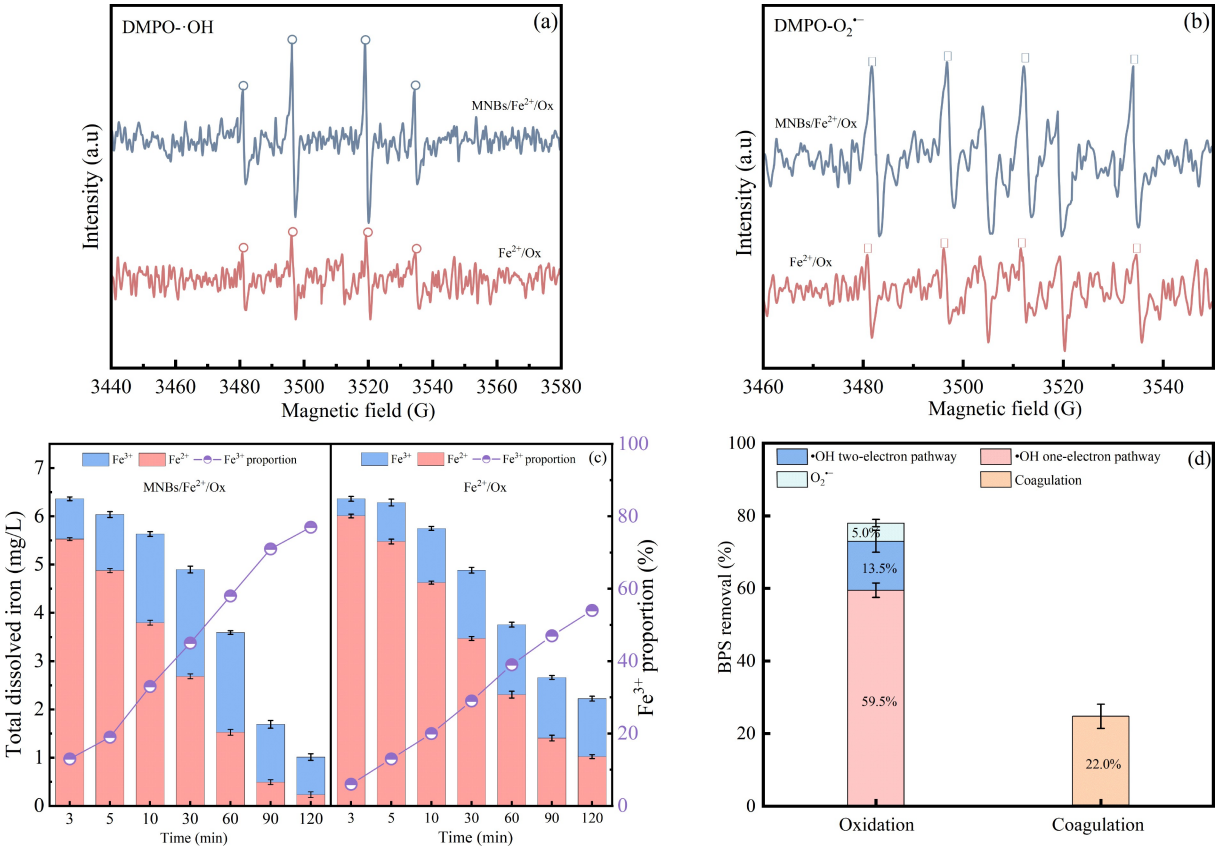

Fig. 3 EPR spectra of DMPO spin traps for ·OH (a) and $O_2^{\bullet-}$ (b) in the system with and without MNBs participation; Comparison of Fe^{2+}/Fe^{3+} conversion in systems with and without MNBs (c); Contribution of oxidation and coagulation to BPS degradation (d). (pH = 7.0, $[Fe^{2+}]$ = 0.1mmol/L, [oxalate] = 0.5 mmol/L, BPS = 100 μg/L, Q_g = 10 mL/min, t = 90 s, [TBA] = 1.5 mmol/L, [PBQ] = 1.5 mmol/L).

$Fe_3(OH)_4^{5+}$ polynuclear iron hydroxide complexes, respectively (Yang et al., 2021; 2023; Zhang et al., 2024). Although there was no difference between the MNBs/Fe^{2+}/Ox and Fe^{2+}/Ox systems in terms of iron species, the peak intensity of the hydrolysis products was significantly elevated when MNBs were involved in the system. In addition, the data in Figs. 4(c) and 4(d) showed that the concentration of $FeOH^{2+}$ and $Fe(OH)_2^+$ were significantly higher in the presence of MNBs in the system than in the absence of MNBs. The above results distinctly indicated that the addition of MNBs played a significant role in the enhancement of coagulation.

The coagulation effect in the system was closely related to the floc properties (Zhang et al., 2024). The influence of MNB involvement on floc properties during floc formation in the MNBs/Fe^{2+}/Ox system suggested that the involvement of MNB in this system played a role in enhancing coagulation. As shown in Figs. S11 and S12, when there were MNBs involved in the system, the flocs formed after the reaction were large and flaky, while when there were no MNBs in the system, the flocs were fine and unaggregated. Besides, the computational analysis of the two-dimensional fractal dimension (D_f) of the flocs and the results of the particle size detection analysis showed (shown in Fig. S13) that the flocs formed in the system with the participation of MNBs had larger particle sizes and D_f, which indicated that the flocs formed had a higher degree of densification. Meanwhile, the EDS energy spectrum analysis of the flocs showed (Fig. S14) that the proportion of "S" elements in the flocs was significantly higher when MNBs were involved than when they were not and that the flocs generated in the system might have a certain sweeping ability (Dong et al., 2015; Sun et al., 2015), and the sweeping effect was more pronounced when the flocs formed were larger.

According to the above results, Figure 5 provides the main removal mechanism for the degradation of BPS by the MNBs/Fe^{2+}/Ox system, highlighting the collaborative action between the oxidation and

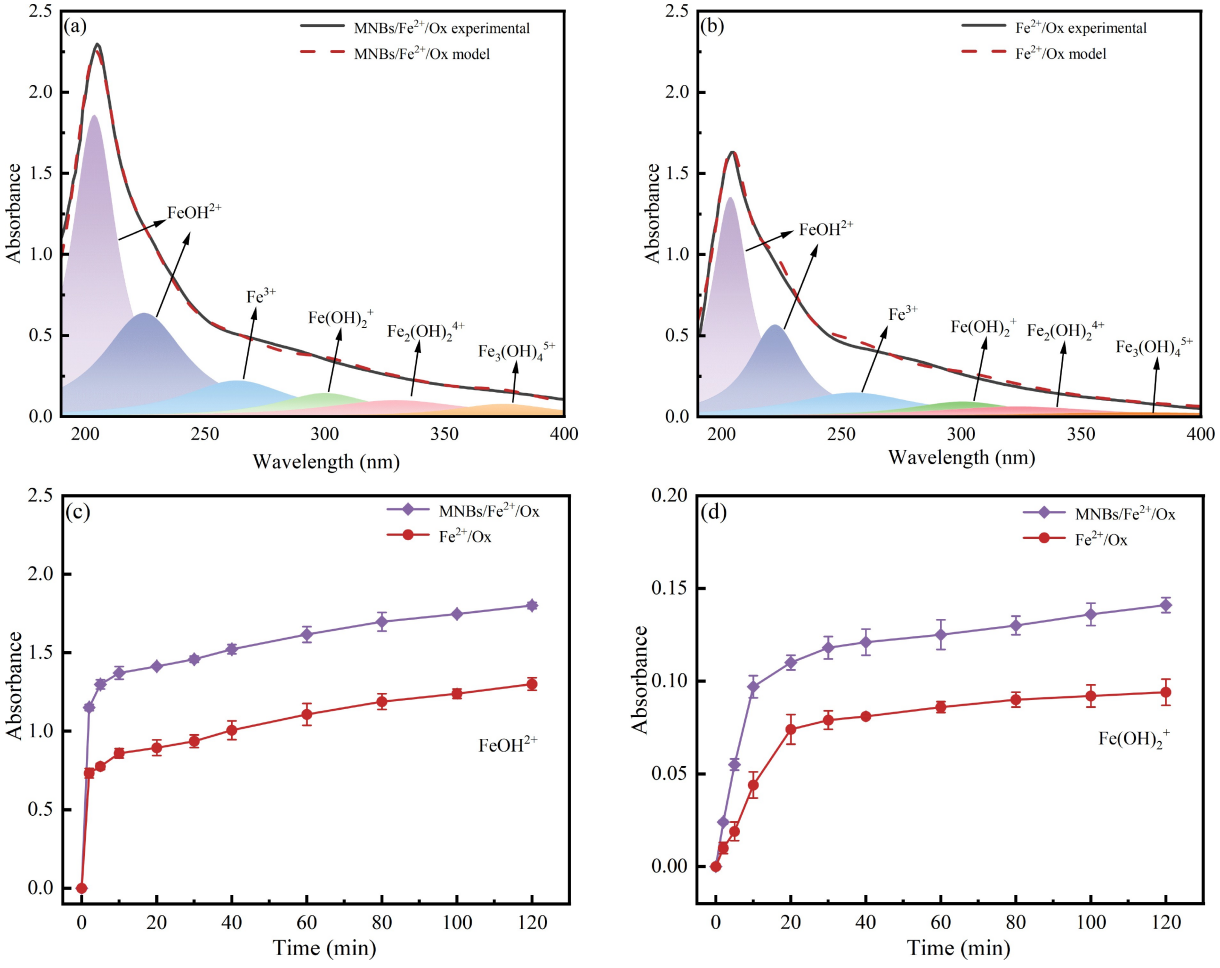

Fig. 4 UV-Vis Spectroscopy of Fe^{3+} hydrolysis products in the System with (a) and without (b) the involvement of MNBs; Variation of $FeOH^{2+}$ (c) and $Fe(OH)_2^+$ (d) in the system with and without the participation of MNBs. (pH = 7.0, $[Fe^{2+}]$ = 0.1 mmol/L, [oxalate] = 0.5 mmol/L, Q_g = 10 mL/min, t = 90 s).

coagulation processes. In the MNBs/Fe^{2+}/Ox system, ·OH and $O_2^{\bullet-}$ were detected as the main ROS species in the system. Moreover, the engagement of MNBs could significantly promote the production of ·OH and $O_2^{\bullet-}$; thus, the involvement of MNBs played an obvious role in enhancing the oxidation. While promoting the generation of ROS, MNBs also accelerated the oxidation of Fe^{2+} and the *in situ* and sequential generation of Fe^{3+}. The continuous conversion of Fe^{2+} to Fe^{3+} led to the generation of mononuclear iron hydroxide and polynuclear iron hydroxide, which were significantly increased in concentration when MNBs were involved. Therefore, the participation of MNBs significantly enhanced the coagulation capability of the system. Overall, in the MNBs/Fe^{2+}/Ox system, MNBs could not only enhance the oxidation, but also the coagulation and the ROS oxidation synergized with the Fe^{3+} coagulation process to effectively degrade the BPS.

3.4 Factors affecting BPS degradation

It has been shown that the Fe^{2+}/Ox system has different oxidation mechanisms under different acid-base conditions (Lee et al., 2014; Yuan et al., 2019). At higher pH conditions, it was not beneficial for the Fe^{2+}/Ox system to generate active species to degrade the contaminants. Therefore, the degradation mechanism of BPS by MNBs/Fe^{2+}/Ox system at different pH conditions was bound to be different. Various anions and cations, large organic matter like humic acid (HA), and small organic acids such as citric acid (CA) were often present in the actual environment. These co-existing substances can affect the degradation of BPS by MNBs/Fe^{2+}/Ox system. However, the effects of these environmental co-existing components on the degradation of BPS by MNBs/Fe^{2+}/Ox system have not been reported. Therefore, this study investigated the

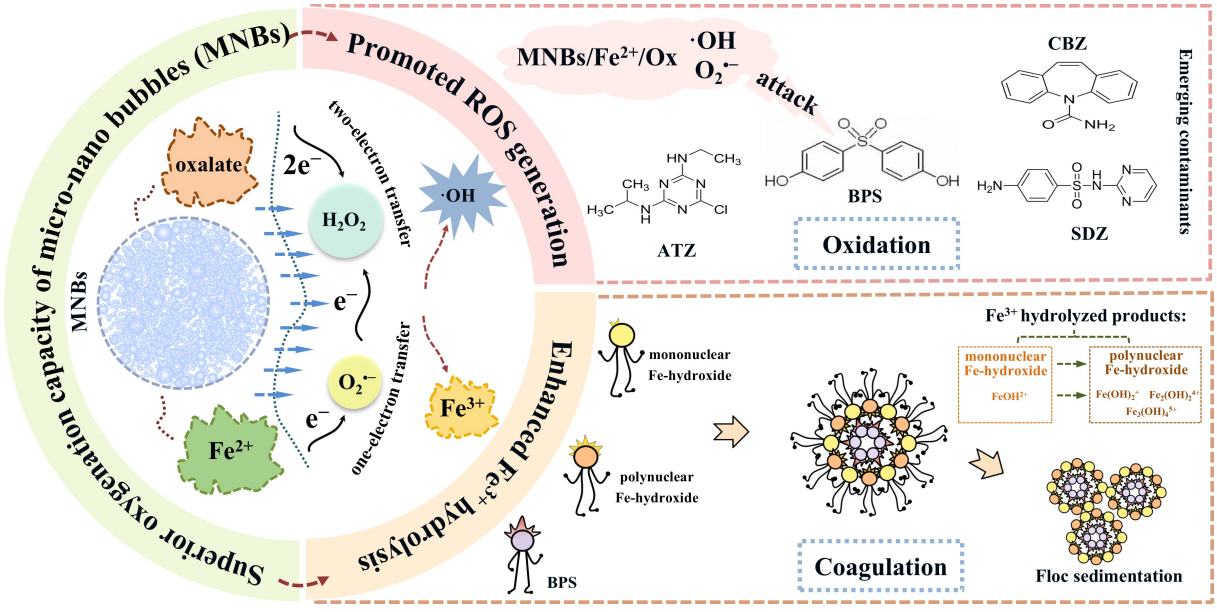

Fig. 5 Degradation mechanism of contaminants in the MNBs/Fe^{2+}/Ox system.

impact of different environmental influences (pH, anions and cations, macromolecules of organic matter, and small molecules of organic acids) on the degradation of BPS by the MNBs/Fe^{2+}/Ox system, the details of which are shown below.

3.4.1 pH

The impact of various pH values (pH range 5.0–9.0) on the degradation of BPS in the MNBs/Fe^{2+}/Ox system was studied. As shown in Fig. 6(a), the degradation of BPS was found to decrease with increasing pH in the experimental pH range. Different solution pH values effect the Fe^{2+}-oxalate complexes speciation (Park et al., 1997; Strathmann and Stone, 2002). As the pH increases, more Fe^{2+} complexes with OH^- ions produce unreactive species such as $Fe^{II}(OH)_2^0$, $Fe^{II}(OH)^+$ and $Fe^{II}(OH)_3^-$, which led to a reduction in the total Fe^{2+}-oxalate complexes content and further inhibits the degradation of BPS (Naka et al., 2006). According to Fig. 6(b), the variations in the concentration of ·OH generated by the MNBs/Fe^{2+}/Ox system at different pH conditions verified the above findings.

3.4.2 Water matrix components

The water matrix components had remarkable influences on the degradation of ECs. The removal of BPS was associated with representative inorganic cations (Ca^{2+}, Mg^{2+}), anions (Cl^-, NO_3^-, CO_3^{2-}, HCO_3^-), macromolecular organic matter HA, and small molecular organic acids CA. As shown in Fig. 7, the addition of Ca^{2+} and Mg^{2+} inhibited the degradation of BPS, mainly because Ca^{2+} and Mg^{2+} would form CaC_2O_4 and MgC_2O_4 sediments with $C_2O_4^{2-}$ (Luo et al., 2009), which inhibited the formed of Fe^{2+}-oxalate complexes, leading to a decrease in ROS amount and the oxidative capacity of the system. The effect of Cl^- and NO_3^- on BPS degradation was negligible within the experimental range. Meanwhile, the degradation of BPS decreased with the increase of CO_3^{2-} and HCO_3^- concentrations. This was attributed to two main reasons: first, CO_3^{2-} and HCO_3^- have a certain reactivity with ·OH (Yang et al., 2016; Long et al., 2023), which in turn led to a decrease in ·OH concentration; second, CO_3^{2-} and HCO_3^- would increase the pH of the system, which was unfavorable for the generation of system ROS, thus reducing the oxidative capacity of the system. Moreover, the addition of HA inhibited the degradation of BPS, which was because HA would compete with BPS for ·OH, and the increase in the concentration of HA would significantly reduce the ·OH concentration in the reaction system (Fig. S15(a)). CA addition promoted the production of ·OH and the degradation of BPS in the process of reaction. When the CA was raised from 0 to 1.0 mmol/L, the ·OH concentration increased about 1.5 times (Fig. S15(b)). That is because CA is also an organic ligand that reacts with Fe^{2+} to form Fe^{2+}-citric acid complexes, which promotes the production of more reactive species in the system and inhibits the formation of non-reactive species (Pham and Waite, 2008; Zhang and Zhou, 2019; Ahile et al., 2020).

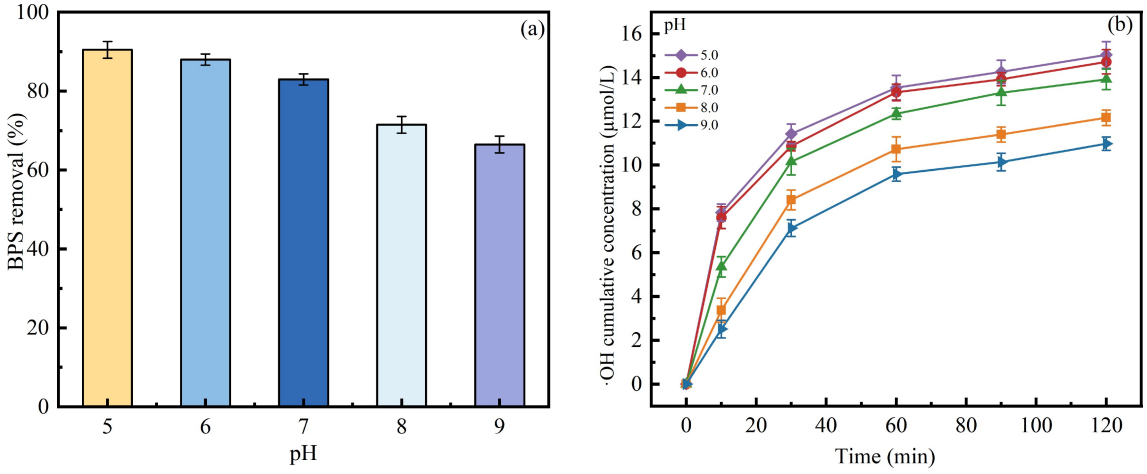

Fig. 6 Effect of pH on BPS degradation (a) and ·OH concentration (b). (pH = 7.0, [Fe^{2+}] = 0.1 mmol/L, [oxalate] = 0.5 mmol/L, BPS = 100 μg/L, Q_g = 10 mL/min, t = 90 s).

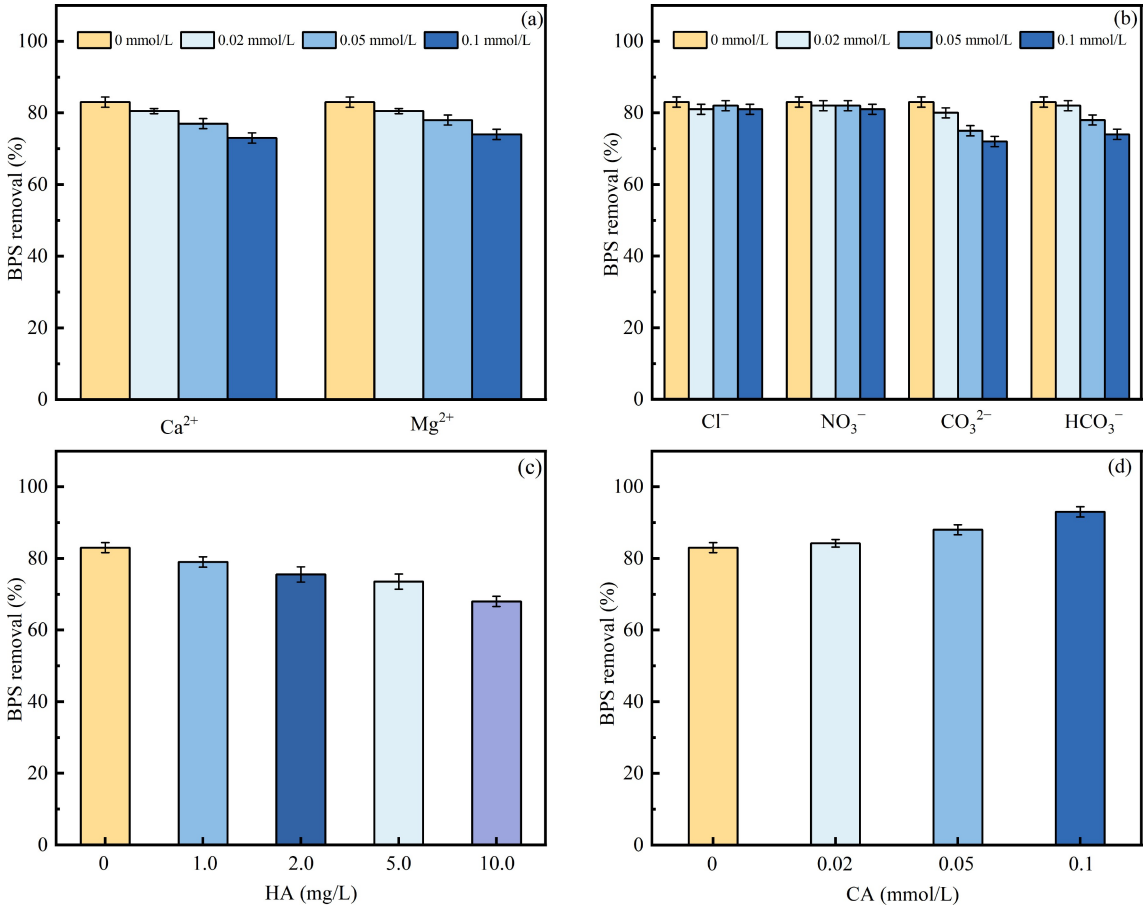

Fig. 7 Effect of water matrix on BPS degradation: coexisting cations (a); coexisting anions (b); HA (c); CA (d). (pH = 7.0, [Fe^{2+}] = 0.1 mmol/L, [oxalate] = 0.5 mmol/L, BPS = 100 μg/L, Q_g = 10 mL/min, t = 90 s).

3.5 Transformation products and degradation mechanisms of BPS

The degradation intermediates of BPS in the MNBs/Fe^{2+}/Ox system were detected and analyzed by LC-MS to obtain a more comprehensive understanding of the degradation process of BPS in the MNBs/Fe^{2+}/Ox system. A total of 20 transformation products (TPs)

of BPS were identified, with hydroxyl and sulfonyl groups present in most of the structures, as listed in Table S2. Based on the comparison between the transformation products detected in this study and previous literature, this study proposed a potential pathway for BPS degradation in the MNBs/Fe^{2+}/Ox system. As shown in Fig. 8, there were two degradation pathways of BPS in the MNBs/Fe^{2+}/Ox system.

First pathway: the active species ·OH produced in the system attacked the two benzene rings of BPS. BPS underwent hydroxylation on the benzene ring in the presence of ·OH, which occurred mainly on the neighboring carbon of the hydroxyl group and yielded the hydroxylation products of BPS, 4-((4-hydroxyphenyl)sulfonyl)benzene-1,2-diol (TP1) and 4,4'-sulfonylbis(benzene-1,2-diol) (TP2) (Lee et al., 2023; Nejumal et al., 2023). Subsequently, TP1 and TP2 reacted in a ring-opening reaction to form the product 3,3′-(sulfonyldimethylenediyl)dipentan-3-ol (TP3). TP2 could also be stripped of SO_2 by an attack on the S-C bond between the sulfur atom and the two neighboring carbon atoms by a ROS substance resulting in breakage to produce 3,3′,4,4'-tetrahydroxybiphenyl (TP4) and TP4 by a further ring-opening reaction to produce 4-hexylresorcinol (TP5) or 7-oxododecan-11-enoic acid (TP6).

Second pathway: ROS attacked the electron-rich sulfur center, causing one of the S-C bonds to break. This reaction released hydroxybenzenesulfonic acid (TP7) and phenol (TP16) (Liu et al., 2019; Chen et al., 2024). TP7 could undergo a ring-opening reaction to form thiodipropionic acid (TP13), diallyl sulfone (TP14), and 6-hydroxyhexane-1-sulfonic acid (TP15), or it could be further oxidized to form 4-sulfobenzoic acid (TP8) and 4-sulfobenzaldehyde (TP9). The S-C bonds in TP8 and TP9 were broken to form benzoic acid (TP10), benzaldehyde (TP11), and sulfuric acid (TP12) (Frankowski et al., 2021; Nejumal et al., 2023). TP16 generated the degradation product hexahydroxybenzene (TP17) by the addition of hydroxyl groups, and TP17 underwent a ring-opening reaction to generate adipic acid (TP18) and 2-hydroxyadipic acid (TP19) or an oxidative reaction to generate o-benzoquinone (TP20) (Chen et al., 2024). As the reaction continues, these products may be further decomposed and finally mineralized to CO_2 and H_2O.

4 Conclusions

Dissolved oxygen concentration plays a vital role in the oxidizing effect of the Fe^{2+}/Ox system, and one of the characteristics of MNBs is that it has a remarkable oxygenating effect. Therefore, this study proposed the combination of MNBs with the Fe^{2+}/Ox system for the removal of ECs to investigate the enhancement effect and mechanism of MNBs on the degradation of contaminants by the Fe^{2+}/Ox system. The specific conclusions were as follows:

1) The presence of MNBs could significantly enhance

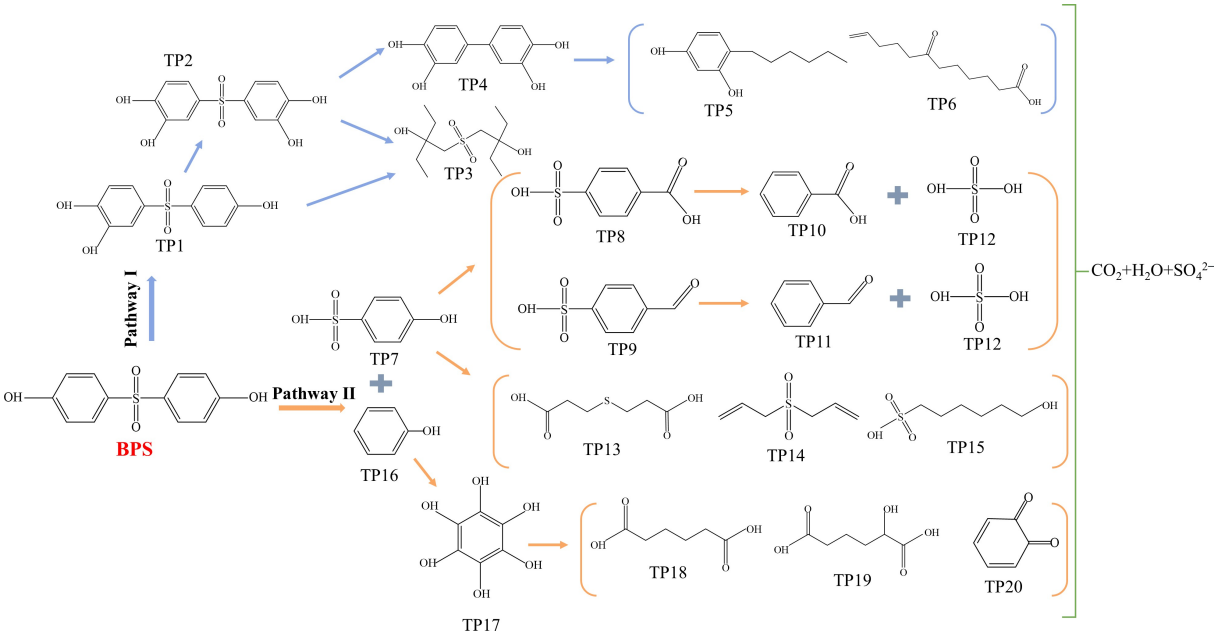

Fig. 8 Degradation pathways of BPS in the MNBs/Fe^{2+}/Ox system.

the degradation efficiency of BPS in the Fe^{2+}/Ox system. The degradation rate of BPS in the MNBs/Fe^{2+}/Ox system mainly depended on the concentration of $Fe^{II}(Ox)_2^{2-}$, and the extent of degradation was jointly decided by $Fe^{II}(Ox)_2^{2-}$ and $Fe^{II}(Ox)^0$ together.

2) Regarding the mechanism of BPS degradation by MNBs/Fe^{2+}/Ox systems, it was determined the role of MNBs in enhancing oxidation and coagulation. In the MNBs/Fe^{2+}/Ox system, ·OH and $O_2^{\bullet-}$ were the main ROS produced in the system. Oxidation played about 78% of the role in the degradation of BPS. Significantly, this oxidation could also promote *in situ* and sequential generation of mononuclear and polynuclear iron hydroxide complexes in the system, greatly contributing to BPS removal by coagulation. In particular, the contribution of coagulation to BPS degradation was about 22%.

3) This study systematically assessed the effects of pH and water matrix components on the removal of BPS. Higher pH was unfavorable for ROS generation and BPS removal. In the water matrix components, high concentrations of Ca^{2+} and Mg^{2+} would inhibit the formation of Fe^{2+}-oxalate complexes. CO_3^{2-} and HCO_3^- would compete with BPS for ·OH and simultaneously lead to an increase in the pH of the reaction system, which was unfavorable for the generation of ·OH.

Conflict of Interests The authors declare that they have no known competing financial interests or personal relationships that could have appeared to influence the work reported in this paper.

Acknowledgements This study was financially supported by the National Natural Science Foundation of China (Nos. 52470014 and 52370100) and the Department of Education of Gansu Province (China): Major Cultivation Project of Scientific Research Innovation Platform in University (No. 2024CXPT-14).

Electronic Supplementary Material Supplementary material is available in the online version of this article at https://doi.org/10.1007/s11783-025-1986-7 and is accessible for authorized users.

References

Agarwal A, Ng W J, Liu Y (2011). Principle and applications of microbubble and nanobubble technology for water treatment. Chemosphere, 84(9): 1175–1180

Ahile U J, Wuana R A, Itodo A U, Sha'ato R, Dantas R F (2020). A review on the use of chelating agents as an alternative to promote photo-Fenton at neutral pH: current trends, knowledge gap and future studies. Science of the Total Environment, 710: 134872

Anglada J M, Martins-Costa M, Francisco J S, Ruiz-López M F (2015). Interconnection of reactive oxygen species chemistry across the interfaces of atmospheric, environmental, and biological processes. Accounts of Chemical Research, 48(3): 575–583

Atkinson A J, Apul O G, Schneider O, Garcia-Segura S, Westerhoff P (2019). Nanobubble technologies offer opportunities to improve water treatment. Accounts of Chemical Research, 52(5): 1196–1205

Belanzoni P, Bernasconi L, Baerends E J (2009). O_2 activation in a dinuclear Fe(II)/EDTA complex: spin surface crossing as a route to highly reactive Fe(IV)oxo species. Journal of Physical Chemistry A, 113(43): 11926–11937

Chandra I, Jeffrey M J H (2005). A fundamental study of ferric oxalate for dissolving gold in thiosulfate solutions. Hydrometallurgy, 77(3−4): 191–201

Chen K, Zhu G, Huang X, Huang X, Xu Y, Pang H, Luo C, Lu J, Zhang Z (2024). New insights into degradation of emerging contaminants by S(IV)/Fe(VI) system in neutral water: performance enhancement, reaction mechanisms and toxicity assessment. Separation and Purification Technology, 328: 125112

Chen N, Geng M, Huang D, Tan M, Li Z, Liu G, Zhu C, Fang G, Zhou D (2022). Hydroxyl radical formation during oxygen-mediated oxidation of ferrous iron on mineral surface: dependence on mineral identity. Journal of Hazardous Materials, 434: 128861

Chen N, Huang D, Liu G, Chu L, Fang G, Zhu C, Zhou D, Gao J (2021). Active iron species driven hydroxyl radicals formation in oxygenation of different paddy soils: implications to polycyclic aromatic hydrocarbons degradation. Water Research, 203: 117484

Coleman R E, Boulton R B, Stuchebrukhov A A (2020). Kinetics of autoxidation of tartaric acid in presence of iron. Journal of Chemical Physics, 153(6): 064503

Dong H Y, Gao B Y, Yue Q Y, Wang Y, Li Q (2015). Effect of pH on floc properties and membrane fouling in coagulation-ultrafiltration process with ferric chloride and polyferric chloride. Chemosphere, 130: 90–97

Fan J H, Liu X, Ma L M (2015). EDTA enhanced degradation of 4-bromophenol by Al^0-Fe^0-O_2 system. Chemical Engineering Journal, 263: 71–82

Frankowski R, Płatkiewicz J, Stanisz E, Grześkowiak T, Zgoła-Grześkowiak A (2021). Biodegradation and photo-Fenton degradation of bisphenol A, bisphenol S and fluconazole in water. Environmental Pollution, 289: 117947

Haris S, Qiu X, Klammler H, Mohamed M M A (2020). The use of micro-nano bubbles in groundwater remediation: a comprehensive review. Groundwater for Sustainable Development, 11: 100463

Jiménez C, Sáez C, Martínez F, Cañizares P, Rodrigo M A (2012). Electrochemical dosing of iron and aluminum in continuous processes: a key step to explain electro-coagulation processes. Separation and Purification Technology, 98: 102–108

Jones A M, Griffin P J, Waite T D (2015). Ferrous iron oxidation by

molecular oxygen under acidic conditions: the effect of citrate, EDTA and fulvic acid. Geochimica et Cosmochimica Acta, 160: 117–131

Keenan C R, Sedlak D L (2008a). Factors affecting the yield of oxidants from the reaction of nanoparticulate zero-valent iron and oxygen. Environmental Science & Technology, 42(4): 1262–1267

Keenan C R, Sedlak D L (2008b). Ligand-enhanced reactive oxidant generation by nanoparticulate zero-valent iron and oxygen. Environmental Science & Technology, 42(18): 6936–6941

Lee J, Eom S, Sohn S, Kim T, Zoh K D (2023). Degradation of bisphenol A, bisphenol S, and bisphenol AF in the UV-LED/chlorine reaction: effect of pH on the kinetics, transformation products, and degradation pathway. Chemical Engineering Journal, 470: 144041

Lee J, Kim J, Choi W (2014). Oxidation of aquatic pollutants by ferrous–oxalate complexes under dark aerobic conditions. Journal of Hazardous Materials, 274: 79–86

Li H, Hu L, Song D, Lin F (2014). Characteristics of micro-nano bubbles and potential application in groundwater bioremediation. Water Environment Research, 86(9): 844–851

Li J, Cassol G S, Zhao J, Sato Y, Jing B, Zhang Y, Shang C, Yang X, Ao Z, Chen G, et al. (2022). Superfast degradation of micropollutants in water by reactive species generated from the reaction between chlorine dioxide and sulfite. Water Research, 222: 118886

Li Q, Li F T (2021). Recent advances in molecular oxygen activation via photocatalysis and its application in oxidation reactions. Chemical Engineering Journal, 421: 129915

Liu Y, Guo H, Zhang Y, Cheng X, Zhou P, Wang J, Li W (2019). Fe@C carbonized resin for peroxymonosulfate activation and bisphenol S degradation. Environmental Pollution, 252: 1042–1050

Long X, Luo J, Zhong Z, Zhu Y, Zhang C, Wan J, Zhou H, Zhang B, Xia D (2023). Performance and mechanism of carbamazepine removal by FeS-$S_2O_8^{2-}$ process: experimental investigation and DFT calculations. Frontiers of Environmental Science & Engineering, 17(9): 113

Luo W, Abbas M E, Zhu L, Zhou W, Li K, Tang H, Liu S, Li W (2009). A simple fluorescent probe for the determination of dissolved oxygen based on the catalytic activation of oxygen by iron(II) chelates. Analytica Chimica Acta, 640(1−2): 63–67

Metz M, Solomon E I (2001). Dioxygen binding to deoxyhemocyanin: electronic structure and mechanism of the spin-forbidden two-electron reduction of O_2. Journal of the American Chemical Society, 123(21): 4938–4950

Minella M, De Laurentiis E, Maurino V, Minero C, Vione D (2015). Dark production of hydroxyl radicals by aeration of anoxic lake water. Science of the Total Environment, 527–528: 322–327

Naka D, Kim D, Strathmann T J (2006). Abiotic reduction of nitroaromatic compounds by aqueous iron(II)-catechol complexes. Environmental Science & Technology, 40(9): 3006–3012

Nejumal K K, Satayev M I, Rayaroth M P, Arun P, Dineep D, Aravind U K, Azimov A M, Aravindakumar C T (2023). Degradation studies of bisphenol S by ultrasound activated persulfate in aqueous medium. Ultrasonics Sonochemistry, 101: 106700

Noradoun C E, Cheng I F (2005). EDTA degradation induced by oxygen activation in a zerovalent iron/air/water system. Environmental Science & Technology, 39(18): 7158–7163

Ouyang Z Z, Yang C, He J H, Yao Q, Zhang B J, Wang H M, Jiang Y, Zhou J N, Deng Y R, Liu Y J, et al. (2020). Homogeneous photocatalytic degradation of sulfamethazine induced by Fe (III)-carboxylate complexes: kinetics, mechanism and products. Chemical Engineering Journal, 402: 126122

Page S E, Kling G W, Sander M, Harrold K H, Logan J R, Mcneill K, Cory R M (2013). Dark formation of hydroxyl radical in arctic soil and surface waters. Environmental Science & Technology, 47(22): 12860–12867

Park J S, Wood P M, Davies M J, Gilbert B C, Whitwood A C (1997). A kinetic and ESR investigation of iron(II) oxalate oxidation by hydrogen peroxide and dioxygen as a source of hydroxyl radicals. Free Radical Research, 27(5): 447–458

Pham A N, Waite T D (2008). Oxygenation of Fe(II) in the presence of citrate in aqueous solutions at pH 6.0–8.0 and 25 °C: interpretation from an Fe(II)/citrate speciation perspective. Journal of Physical Chemistry A, 112(4): 643–651

Sakr M, Mohamed M M, Maraqa M A, Hamouda M A, Aly Hassan A, Ali J, Jung J (2022). A critical review of the recent developments in micro-nano bubbles applications for domestic and industrial wastewater treatment. Alexandria Engineering Journal, 61(8): 6591–6612

Schwarzenbach R P, Escher B I, Fenner K, Hofstetter T B, Johnson C A, Von Gunten U, Wehrli B (2006). The challenge of micropollutants in aquatic systems. Science, 313(5790): 1072–1077

Strathmann T J, Stone A T (2002). Reduction of oxamyl and related pesticides by Fe(II): influence of organic ligands and natural organic matter. Environmental Science & Technology, 36(23): 5172–5183

Sun S L, Bu F, Huang X, Zhao S, Dong H Y, Gao B Y, Yue Q Y, Feng L J, Wang Y, Li Q (2015). Effects of epichlorohydrin-dimethylamine on coagulation and membrane performance of ferric chloride in coagulation-ultrafiltration hybrid process. Chemical Engineering Journal, 280: 634–642

Sun Y D, Guo S Q, Fan L L, Cai J Y, Han W G, Zhang F Y (2024). Molecular oxygen activation in photocatalysis: generation, detection and application. Surfaces and Interfaces, 46: 104033

Takahashi M (2005). Zeta potential of microbubbles in aqueous solutions: electrical properties of the gas-water interface. Journal of Physical Chemistry B, 109(46): 21858–21864

Tong M, Yuan S, Ma S, Jin M, Liu D, Cheng D, Liu X, Gan Y, Wang Y (2016). Production of abundant hydroxyl radicals from oxygenation of subsurface sediments. Environmental Science & Technology, 50(1): 214–221

Villegas-Guzman P, Giannakis S, Torres-Palma R A, Pulgarin C (2017). Remarkable enhancement of bacterial inactivation in wastewater through promotion of solar photo-Fenton at near-neutral pH by natural organic acids. Applied Catalysis B: Environmental, 205: 219–227

Wang T, Yang C, Sun P, Wang M, Lin F, Fiallos M, Khu S T (2024a). Generation mechanism of hydroxyl free radicals in micro-nanobubbles water and its prospect in drinking water. Processes, 12(4): 683

Wang Y, Deng Y, Yao L, Yang X (2024b). Colloid-bound radicals formed in NOM-enhanced Fe(III)/peroxymonosulfate process accelerate the degradation of trace organic contaminants in water. Water Research, 248: 120880

Wu B D, Zhang G Y, Zhang L, Song X J, Zhang S J, Zhu B Z (2020). Key factors in the ligand effects on the photo redox cycling of aqueous iron species. Geochimica et Cosmochimica Acta, 281: 1–11

Xie W J, Zhang P, Liao W J, Tong M, Yuan S H (2021). Ligand-enhanced electron utilization for trichloroethylene degradation by •OH during sediment oxygenation. Environmental Science & Technology, 55(10): 7044–7051

Yang G, Cheng Z Y, Bao H Z, Zhang L B, Zhang H W, Jia H, Wang J (2022). Mechanistic insight of weak magnetic field trigger transformation of amorphous Fe(III)-(oxy)hydroxide for enhanced Ferrate(VI) towards selective removal of natural organic matter. Chemosphere, 303: 134967

Yang G, Li J, Cheng Z Y, Qin Q W, Zhang H W, Lu N, Wang J (2023). Revealing key meso-particles responsible for irreversible membrane fouling in an integrated oxidation-coagulation ultrafiltration system: fouling behavior and interfacial interaction mechanism. Chemical Engineering Journal, 454: 140482

Yang G, Wang J, Zhang H W, Jia H, Zhang Y, Gao F (2021). New insight into quinones triggered ferrate *in-situ* synthesized polynuclear Fe-hydroxyl complex for enhancing interfacial adsorption in highly efficient removal of natural organic matter. Science of the Total Environment, 770: 144844

Yang Y, Pignatello J J, Ma J, Mitch W A (2016). Effect of matrix components on UV/H_2O_2 and UV/$S_2O_8^{2-}$ advanced oxidation processes for trace organic degradation in reverse osmosis brines from municipal wastewater reuse facilities. Water Research, 89: 192–200

Yuan D, Zhang C, Tang S, Li X, Tang J, Rao Y, Wang Z, Zhang Q (2019). Enhancing CaO_2 Fenton-like process by Fe(II)-oxalic acid complexation for organic wastewater treatment. Water Research, 163: 114861

Zhang C, Kong C, Tratnyek P G, Qin C (2022). Generation of reactive oxygen species and degradation of pollutants in the Fe^{2+}/O_2/Tripolyphosphate system: regulated by the concentration ratio of Fe^{2+} and tripolyphosphate. Environmental Science & Technology, 56(7): 4367–4376

Zhang C, Li T, Zhang J, Yan S, Qin C (2019). Degradation of p-nitrophenol using a ferrous-tripolyphosphate complex in the presence of oxygen: the key role of superoxide radicals. Applied Catalysis B: Environmental, 259: 118030

Zhang C, Liu L W, Pan Y W, Qin R, Wang W, Zhou M H, Zhang Y (2025). Detection methodologies and mechanisms of reactive oxygen species generated in Fenton/Fenton-like processes. Separation and Purification Technology, 355: 129578

Zhang Y, Li Z, Yan D, Chen H, Zhang M, Wang J, Yang G (2024). Application of Fe(II)/peroxymonosulfate for efficient alkali lignin wastewater treatment: insight into the synergistic interactions between redox reactions and coagulation. Separation and Purification Technology, 328: 125037

Zhang Y, Zhou M H (2019). A critical review of the application of chelating agents to enable Fenton and 1 Fenton-like reactions at high pH values. Journal of Hazardous Materials, 362: 436–450

Zhou H Y, Sun Q, Wang X, Wang L L, Chen J, Zhang J D, Lu X H (2014). Removal of 2,4-dichlorophenol from contaminated soil by a heterogeneous ZVI/EDTA/Air Fenton-like system. Separation and Purification Technology, 132: 346–353

Zhou S, Nazari S, Hassanzadeh A, Bu X, Ni C, Peng Y, Xie G, He Y (2022). The effect of preparation time and aeration rate on the properties of bulk micro-nanobubble water using hydrodynamic cavitation. Ultrasonics Sonochemistry, 84: 105965

Zimmerman W B, Tesar V, Bandulasena H C H (2011). Towards energy efficient nanobubble generation with fluidic oscillation. Current Opinion in Colloid & Interface Science, 16(4): 350–356